Recirculating Mixed Convection Flows in Rectangular Cavities

Ranganathan Kumar* and Tsorng-Dih Yuan†
Clemson University, Clemson, South Carolina

A numerical investigation is carried out to determine the flow and thermal structures of mixed convective flow in a rectangular cavity. The effect of aiding and opposing buoyancy on the flow in a vertical downward laminar jet is studied for $Re \leq 200$, $-1.0 \leq Ri \leq 0.5$, and $0.5 \leq A \leq 5.0$. Such flow situations occur in enclosure fires, energy storage, and ventilation systems. Results of the velocity profile, temperature distribution, local friction factor, and heat-transfer coefficient are presented for both hot and cold jets. The flow configuration is found to be strongly affected by the positive and negative buoyancy and also by the aspect ratio of the cavity.

Nomenclature

C_f = wall friction factor
C_f^* = $C_f/Re^{1/2}$
g = acceleration of gravity
Gr = Grashof number, $g\beta(T_j - T_w)\ell^3/\nu^2$
h = local heat-transfer coefficient, $q/(T_j - T_w)$
H = height of the cavity
A = nondimensional slot height, H/L
k = thermal conductivity
ℓ = width of the jet
L = horizontal length of the cavity
$\dot{m}$ = mass flow rate
Nu = Nusselt number, $h\ell/k$
Nu^* = $Nu/Re^{1/2}$
p = pressure
P = nondimensional pressure, $(p - p_\infty)\rho v_j^2$
Pr = Prandtl number
q = local heat flux
Re = Reynolds number, $v_j\ell/\nu$
Ri = Richardson number, Gr/Re^2
S = source term
T = thermodynamic temperature
u = velocity component in x direction
U = nondimensional velocity component in x direction, u/v_j
v = velocity component in y direction
V = nondimensional velocity component in y direction, v/v_j
x = coordinate along the lower surface of the cavity
X = nondimensional coordinate, x/ℓ
y = vertical coordinate
Y = nondimensional coordinate, y/ℓ
α = thermal diffusivity
β = thermal expansion coefficient
Γ = diffusion coefficient
θ = nondimensional temperature, $(T - T_w)/(T_j - T_w)$
μ = dynamic viscosity
ν = kinematic viscosity
ρ = density
ϕ = variable

Subscripts

j = slot exit
max = maximum value of the variable
w = impinging surface
∞ = ambient

Introduction

SEVERAL studies have been reported on impinging jets, but very little information is available regarding impinging flows in cavities. This paper reports the study of hot and cold laminar downward jets drawn from one top end of the cavity and discharged to the other top corner. The walls are maintained at constant temperature. This problem is of interest in practical applications such as enclosure fires, solar ponds, energy storage, heat rejection, and ventilation systems.

In an enclosure fire, the buoyancy force opposes the cold jet of fluid flowing downward, resulting in negative buoyancy. Goldman and Jaluria[1] studied the effect of opposing buoyancy on the flow in free and wall jets experimentally. They developed an experimental system to study the downward penetration of such jets in which the buoyancy force opposes the externally induced flow. The penetration distance was quantified by defining it as the vertical distance from the jet inflow to the location where the local temperature excess had dropped to 1% of the inlet temperature excess. Temperature and velocity profiles were also given for a range of buoyancy parameters and Reynolds numbers.

Cha and Jaluria[2,3] directed their efforts toward understanding the effect of thermal buoyancy on the recirculating flow for energy extraction and heat rejection. In this numerical study, the hot fluid was withdrawn at the top and the cold fluid discharged at the bottom of the storage region to preserve the thermal stratification. It was shown that the inflow parameters could be chosen to control the vertical spread and horizontal penetration of the flow. Also, they found that the flow penetrated further into the storage zone in the same-end configuration and flow reversal occurred in the opposite-end configuration.

Prahl et al.[4] and Satyanarayana and Jaluria[5] studied thermal energy discharge into the ambient air-and-water medium that gave rise to negatively buoyant flows. Analytical and experimental studies have been done on negatively buoyant axisymmetric jet by Turner[6] and Seban et al.[7] Turner's[6] model predicted the penetration distance, which compared well with the experimental values, but the flow rates and the velocity and temperature distributions were not predicted accurately by Turner's analysis, as shown by Seban et al.[7] Yuan et al.[8] studied the effect of buoyancy on laminar, heated, two-dimensional jets impinging on an isothermal surface. They considered both

Received July 2, 1987; revision received April 10, 1988.

*Assistant Professor, Department of Mechanical Engineering.
†Graduate Assistant, Department of Mechanical Engineering.

upward- and downward-facing jets. Their work showed that the magnitude of both the friction factor and heat-transfer coefficient on the wall depended on the separation distance between the jet exit and the impinging surface, and that flow separation would occur in the downward-facing flow for large buoyancy parameters, depending on the aspect ratio. In other cavity flows driven by buoyancy and shear, Torrance et al.[9] numerically investigated the fluid motion driven by a moving wall and natural convection.

This study concentrates on the characteristics of both aiding and opposing buoyant flows arising from hot and cold jets impinging from one end of the top corner of the cavity and discharging through the other end. Unlike in the work of Goldman and Jaluria,[1] the top is not left open, and there is no entrainment from the ambient. The four walls are maintained isothermal at the same temperature as the ambient. The jet is uniform at the jet exit and is at a higher or lower temperature than the walls. A steady, laminar, two-dimensional flow is assumed. Velocity and temperature profiles are obtained inside the cavity along with the heat-transfer rates and friction factor on the bottom wall for various aspect ratios, Richardson number (also called buoyancy parameter or mixed convection parameter), and Reynolds number and the physics of the flow analyzed.

Mathematical Formulation

The flow is considered to be two-dimensional, steady, incompressible, and laminar. The initial velocity and temperature profiles are assumed to be uniform, and the jet fluid is isothermal and may be warmer or cooler than the cavity walls, which are maintained at constant temperature T_w. It is assumed that the density variation is accounted for only in the body force term. The physical properties are assumed to be constant. The energy equation is formulated by neglecting the viscous dissipation and the change of temperature due to compression.

Under these foregoing assumptions, the governing conservation equations of mass, momentum, and energy are

$$\frac{\partial u}{\partial x}+\frac{\partial v}{\partial y}=0 \tag{1}$$

$$\frac{\rho u\partial u}{\partial x}+\frac{\rho v\partial u}{\partial y}=\frac{-\partial p}{\partial x}+\mu\left(\frac{\partial^2 u}{\partial x^2}+\frac{\partial^2 u}{\partial y^2}\right) \tag{2}$$

$$\frac{\rho u\partial u}{\partial x}+\frac{\rho v\partial v}{\partial y}=\frac{-\partial p}{\partial y}+\mu\left(\frac{\partial^2 v}{\partial x^2}+\frac{\partial^2 v}{\partial y^2}\right)+\rho g \tag{3}$$

$$\frac{u\partial T}{\partial x}+\frac{v\partial T}{\partial y}=\alpha\left(\frac{\partial^2 T}{\partial x^2}+\frac{\partial^2 T}{\partial y^2}\right) \tag{4}$$

For relatively small change of density with temperature, the body force term in Eq. (3) can be expressed in terms of the ambient conditions using a Boussinesq approximation as

$$\rho g=\rho_\infty g+\rho g\beta(T_\infty-T) \tag{5}$$

The scaling parameters are chosen as v_j, the average velocity at the jet exit, ℓ, the width of the jet, T_j-T_w, the temperature difference between the jet exit and the surface, and ρv_j^2, the characteristic pressure. Nondimensional variables are defined as

$$\begin{aligned} U&=u/v_j\\ V&=v/v_j\\ X&=x/\ell\\ Y&=y/\ell\\ P&=(p-p_\infty)/\rho v_j^2\\ \theta&=(T-T_w)/(T_j-T_w) \end{aligned} \tag{6}$$

Substituting the given nondimensional variables into Eqs. (1–4) and using Eq. (5) results in

$$\frac{\partial U}{\partial X}+\frac{\partial V}{\partial Y}=0 \tag{7}$$

$$\frac{U\partial U}{\partial X}+\frac{V\partial U}{\partial Y}=\frac{-\partial P}{\partial X}+\frac{1}{Re}\left(\frac{\partial^2 U}{\partial X^2}+\frac{\partial^2 U}{\partial Y^2}\right) \tag{8}$$

$$\frac{U\partial V}{\partial X}+\frac{V\partial V}{\partial Y}=\frac{-\partial P}{\partial Y}+\frac{1}{Re}\left(\frac{\partial^2 V}{\partial X^2}+\frac{\partial^2 V}{\partial Y^2}\right)+Ri\theta \tag{9}$$

$$\frac{U\partial T}{\partial X}+\frac{V\partial T}{\partial Y}=\left(\frac{1}{Re\,Pr}\right)\left(\frac{\partial^2 T}{\partial X^2}+\frac{\partial^2 T}{\partial Y^2}\right) \tag{10}$$

The governing parameters as seen from the preceding equations are Reynolds number Re, Richardson number Ri, and Prandtl number Pr. The other relevant parameters in this problem are aspect ratio $A(=H/L)$ and L/ℓ. The boundary conditions are those of impermeable, isothermal walls and are given in nondimensionalized form:

$$\begin{aligned} &U=0;\quad V=-1;\quad \theta=1 \text{ at the jet exit}\\ &U=0;\quad V=0;\quad\ \ \theta=0 \text{ on all walls}\\ &\dot m_{\text{in}}=\dot m_{\text{out}} \end{aligned} \tag{11}$$

The flowfield is subdivided into finite volumes, each of which encloses an imaginary grid node. Scalar variables such as pressure, density, viscosity, and temperature are evaluated at the grid node, while the velocity components are chosen to lie on the control volume faces, where they are used for the mass flow rate computations. The set of governing differential equations is integrated to yield finite-difference equations. These finite-difference equations are then solved together with a pressure correction equation to satisfy the continuity equation. The solution procedure follows that given by Patankar[10] in the program SIMPLE, with the modification recommended by Ván Doormaal and Raithby.[11]

Numerical Procedure

The governing equations are cast in the common form

$$\frac{\partial(U_j\phi)}{\partial X_i}=\partial\left(\frac{\Gamma\partial\phi}{\partial X_i}\right)+S \tag{12}$$

The first term represents the flux of any dependent variable ϕ convected by the mass flow rate ρu_i, the second term represents diffusion, and the last term is the mechanism for generation (or destruction) of ϕ. Whatever cannot be expressed through convection and diffusion terms can be lumped into the last source term. Each variable in the governing equations is given in Table 1 for each of the governing equations.

Equation (12), together with the boundary conditions given in Eq. (11), constitute a set of three coupled nonlinear partial differential equations. The results presented in this study were obtained for 20 × 20, 24 × 24, and 32 × 32 grids, closely spaced in regions of strong gradients of ϕ, i.e., close to the surface. The solution was checked for grid independence.

Table 1 Variables for the general equation

Equation	ϕ	Γ	Source
Mass	1	0	0
x momentum	U	$1/Re$	$-\partial P/\partial X$
y momentum	V	$1/Re$	$-\partial P/\partial Y+(Gr/Re^2)\theta$
Energy	θ	$1/Re\,Pr$	0

The range of flow parameters used in this study is given in Table 2. These parameters also affect the mentioned grid specification. The grid spacing required for each flow pattern was investigated. In summary, for higher values of A, Re, and Ri, a larger grid size and finer grid spacing is required. Thus, the given limits were the minimum amount for the grid independent solutions and were increased as needed. The calculation times for each case ranged from 1 min 30 s for the 18 × 18 grid for 150 iterations to 3 min 10 s for the 32 × 32 grid for 150 iterations using the computer NAS AS/XL-60.

Results and Discussion

The detailed structure of flow in a rectangular cavity in which a downward hot or cold jet impinges from the top left corner as shown in Fig. 1 is analyzed for various Reynolds numbers, Richardson numbers, and aspect ratios. The range of these parameters is given in Table 2. The range of parameters was suitably chosen to avoid transgressing in the turbulent region. No experimental or analytical work in this flow situation has been reported in the literature, and hence, there is no clear knowledge of when and for what combination of parameters the flow becomes turbulent. However, the upper limit of Reynolds number for which the flow stays laminar was not reached in this study. Also, numerical oscillations and divergence would occur if the flow ceases to be steady or laminar.

Since the present results could not be directly compared with available results in the literature, the computational scheme was validated by considering a two-dimensional stagnation flow problem and comparing the results with the exact solution obtained by Howarth.[12] The results were in excellent agreement.

The velocity vectors for no buoyancy (i.e., $Ri = 0$), $A = 1$, and Reynolds numbers of 50, 100, and 200 are given in Fig. 2. For $Re = 50$, a secondary cell is seen to form at the lower left corner, which grows in size as Re is increased. Another cell develops in the bottom right corner, which is clearly visible at $Re = 200$. Due to increased velocities in the case of high Reynolds numbers, the recirculating flow pushes the center of the vortex down slightly. The effect of buoyancy on the flowfield is presented in Fig. 3 for $Ri = 0.1$ and -0.1. The positive Richardson number indicates that the jet is heated, and the negative value represents a cold jet. Here, the jet is heated or

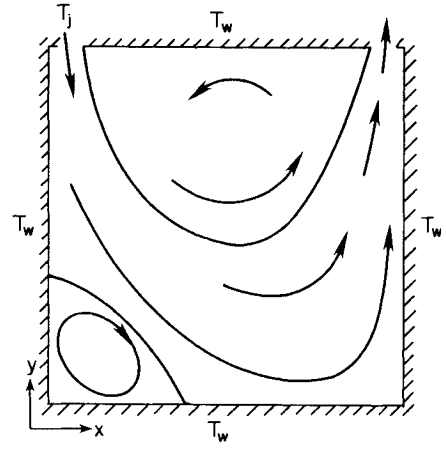

Fig. 1 Rectangular cavity and flow configuration.

Table 2 Ranges of governing parameters

Re	Gr	Ri	Pr	$A(=H/L)$	L/ℓ
50–200	0–5000	−1.0–+0.5	0.7	0.5–5.0	5–8

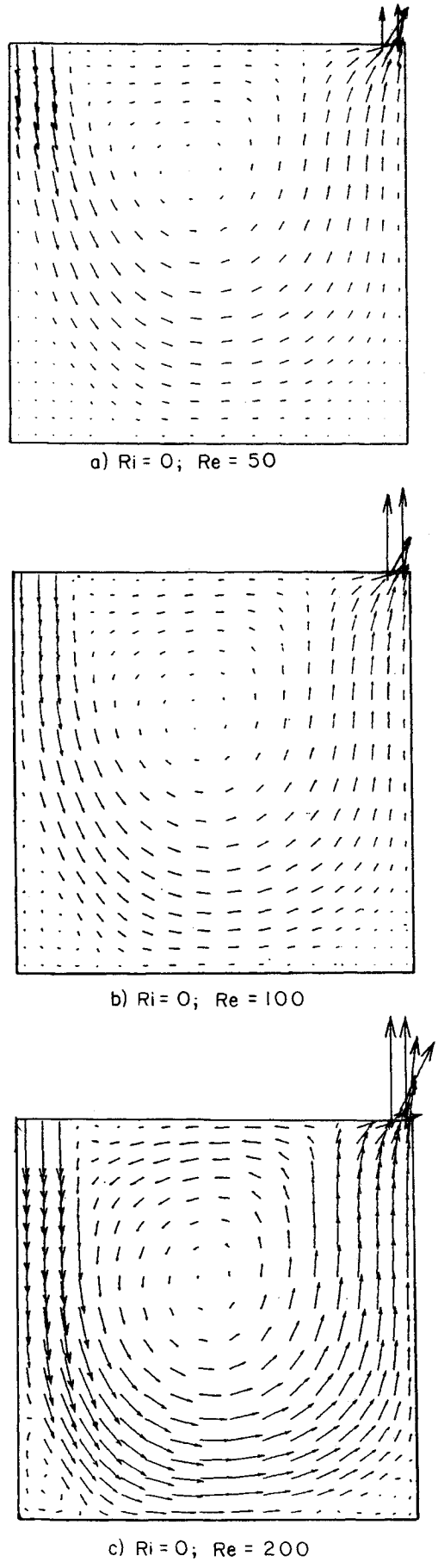

Fig. 2 Flowfield for $A = 1$, $Ri = 0$, and a) $Re = 50$; b) $Re = 100$; and c) $Re = 200$.

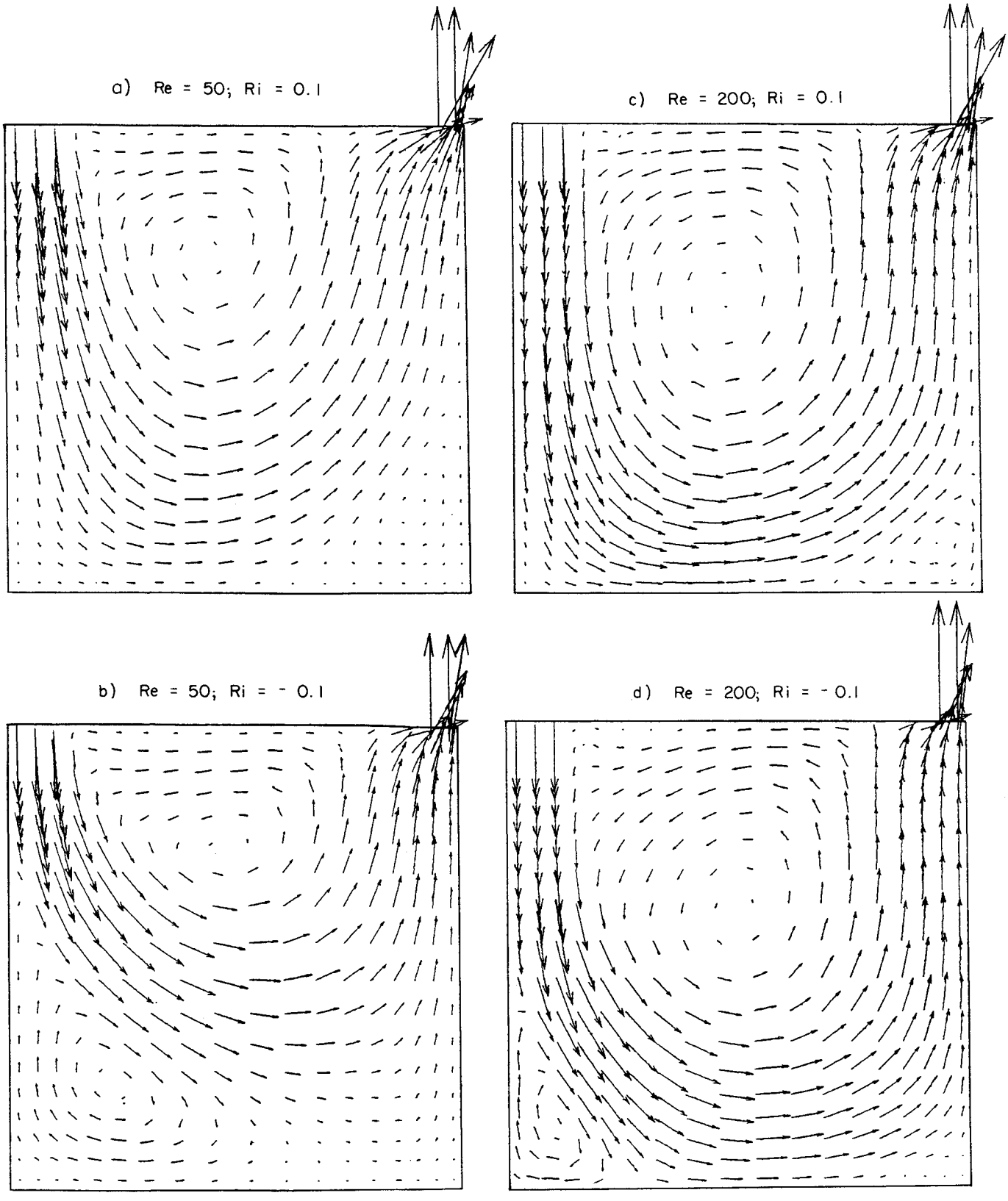

Fig. 3 Flowfield for $A = 1$; a) $Re = 50$, $Ri + 0.1$; b) $Re = 50$, $Ri = -0.1$; c) $Re = 200$, $Ri = 0.1$; and d) $Re = 2000$, $Ri = -0.1$;

cooled relative to the cavity walls, which are maintained at the same constant temperature T_w. For $Ri = 0.1$, the left corner cell completely disappears, the right corner cell increases in size as Re increases, and the streamlines are seen to be skewed more to the right.

The physics of the flow presented in Fig. 3 is interesting and vastly different, depending on the temperature of the jet with respect to the wall. The hot jet penetrates all the way to the lower wall since the buoyancy parameter Ri is low. There is no counterflow in the left corner as the wall is colder than the fluid, and hence, the fluid near the left corner is denser than the fluid that is penetrating. After the fluid impinges on the bottom wall, the buoyancy of the jet and the acceleration of the fluid around the right corner turns the flow upwards, thus giving birth to a secondary cell at the bottom right corner. The temperature distribution given in Fig. 4 confirms the preceding

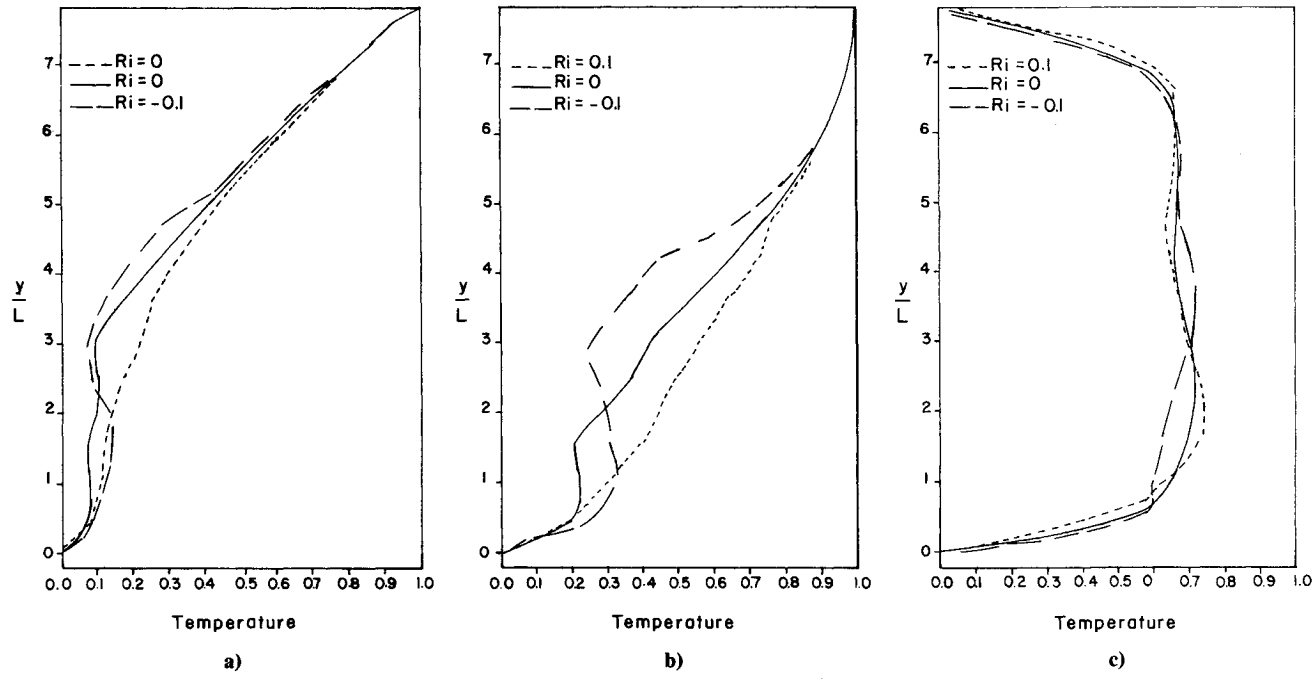

Fig. 4 Effect of Richardson number on temperature profile for $A = 1$, $Re = 100$, and a) $x/\ell = 0.167$; b) $x/\ell = 0.5$; and c) $x/\ell = 3.5$.

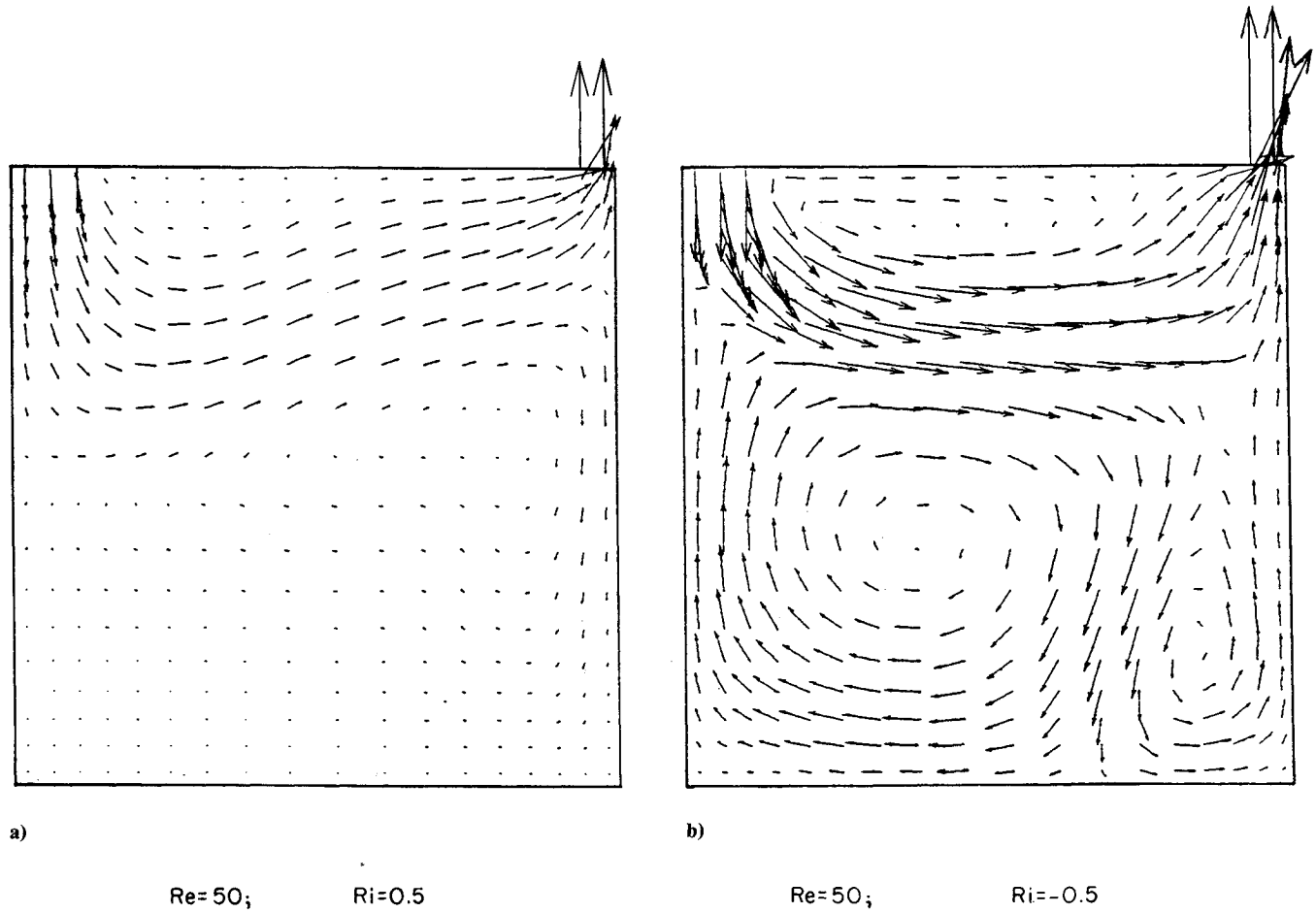

Fig. 5 Flow pattern for high buoyancy parameter for $A = 1$, $Re = 50$, and a) $Ri = 0.5$; and b) $Ri = -0.5$.

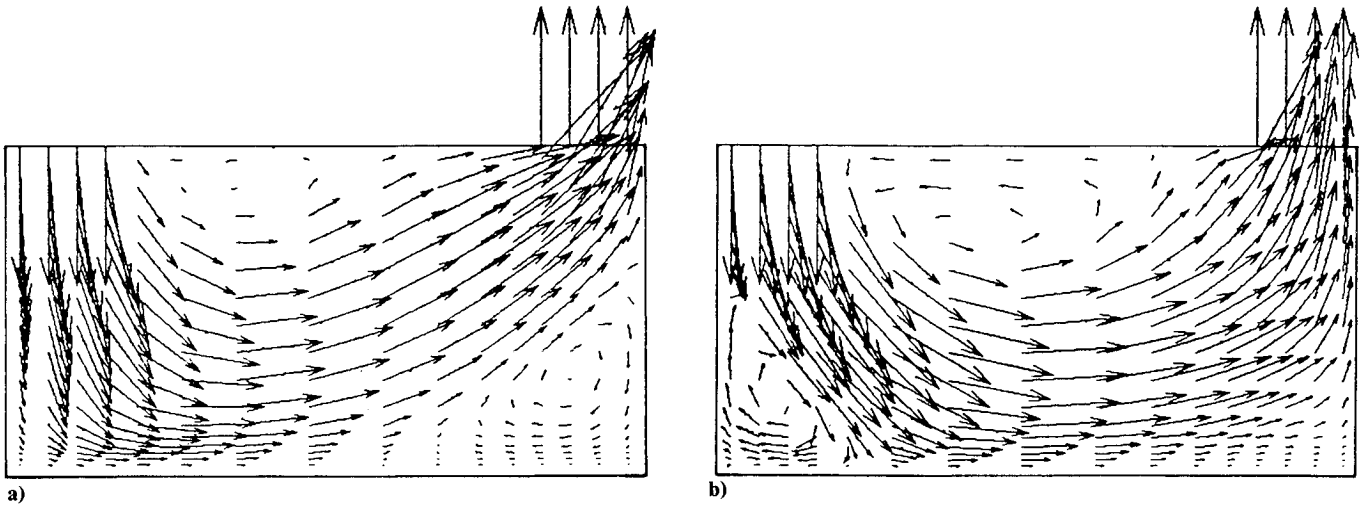

Fig. 6 Flowfield for $Re = 50$, $A = 0.5$, and a) $Ri = 0.5$; and b) $Ri = -0.5$.

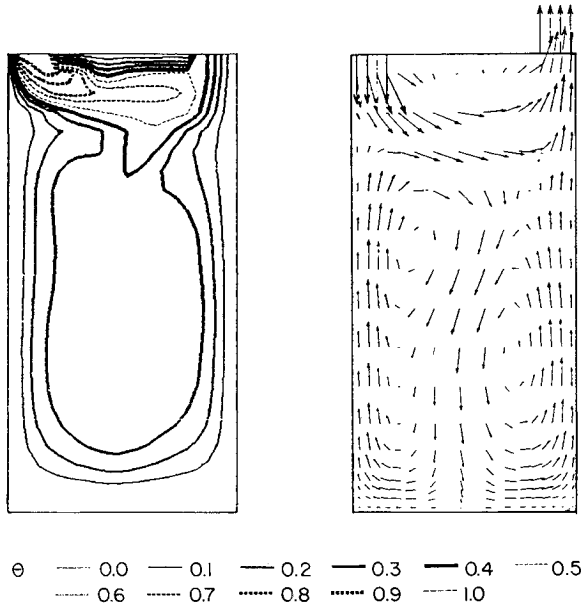

Fig. 7 Isotherms and velocity vectors for $Re = 50$, $A = 2$, and $Ri = -0.5$.

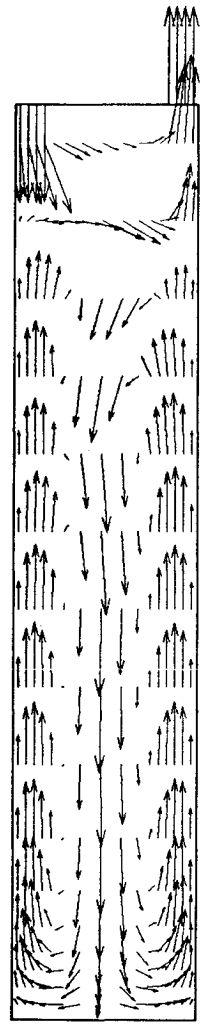

Fig. 8 Flowfield for $Re = 50$, $A = 5$, and $Ri = -0.5$.

observation. In the bottom of the cavity, i.e., below $y/L = 0.4$, the temperature of the fluid is seen to increase along the x direction until the location where the jet turns upwards. The fluid in the secondary cell is relatively cold due to the presence of the cold wall.

In the case of a cold jet for the same Reynolds number of 100 and the same absolute value of Richardson number ($Ri = -0.1$), the flow structure adjusts itself to give rise to a secondary cell in the bottom left corner (Fig. 3). In this case, the walls are warmer than the incoming jet. The fluid particles closer to the left wall rise due to buoyancy, but they are unable to penetrate higher up in the cavity due to the momentum of the cold jet. Hence, they recirculate to form a clockwise cell. This is a mixed convection opposing flow situation. The temperature profile in Fig. 4 for $Ri = 0.1$ at $x/L = 0.5$ (inside the secondary cell) shows an S-shaped curve representing the penetrating warm parcel of fluid arising from the walls, cooled in turn by the incoming jet. Such a characteristic in temperature is also seen for $x/L = 0.167$. As the fluid flows along the horizontal wall and accelerates around the bottom right corner, it aids the buoyant penetrating fluid arising from the right wall, and hence, no secondary cell appears in the right corner when the impinging jet is cold. Figure 4 depicts the relative magnitudes of nondimensional temperatures when buoyancy is taken into account and compares the results for no buoyancy. It should be noted that in the case of cold jets (negative Richardson numbers), decreasing nondimensional temperatures indicate that the fluid is getting warmer. The effect of buoyancy is seen to be significant only in the bottom corners of the cavity. In the core, the error in temperature is not considerable.

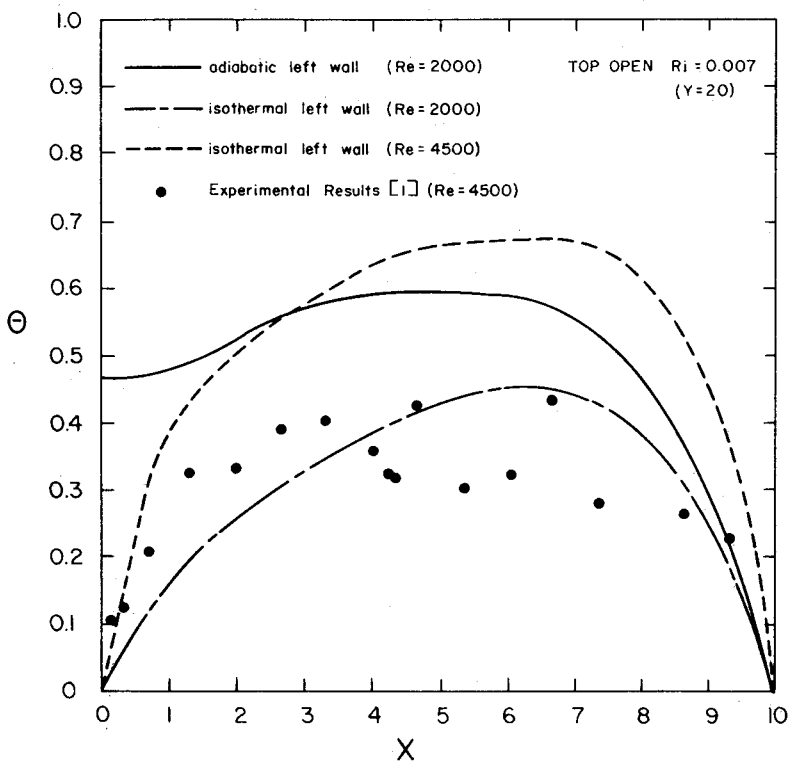

Fig. 9 Comparison of temperature profile with experimental results.

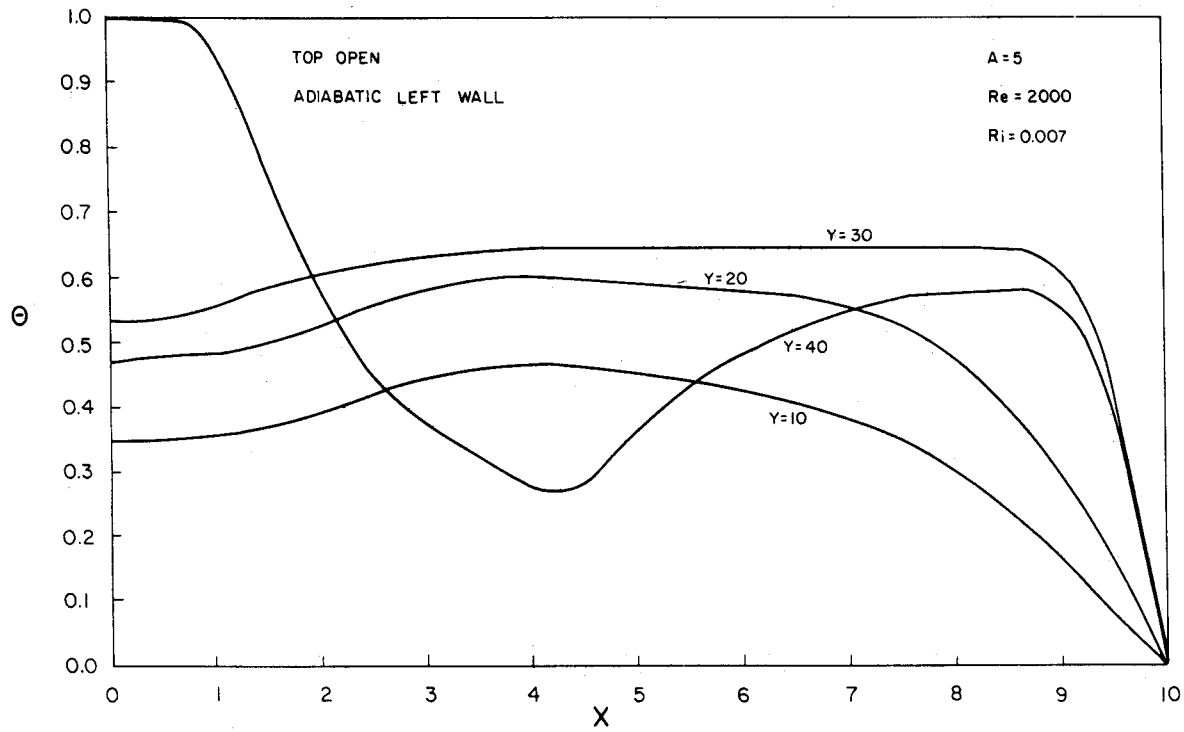

Fig. 10 Temperature profile for an adiabatic left wall at different vertical positions.

The velocity vectors for the case of $Ri = -0.1$ and Reynolds number of 50 and 200 (Figs. 3b and 3d) show that as Re is increased, the buoyancy effect is not dominant, since the Richardson number remains the same. Hence, the cold jet is able to penetrate deeper into the cavity and is faster due to increased momentum, and the secondary cell in the bottom left corner diminishes in size. Such a reduction in cell size is not noticeable for $Ri = 0.1$, when Re is increased.

The effect of high buoyancy parameter is shown in Fig. 5. For $A = 1$, $Re = 50$, and $Ri = 0.5$, strong buoyancy and low Reynolds number prevent the flow from penetrating deep into the cavity. A mild recirculating bubble is seen near the top wall to the right of which the flow forms a strong wall jet region leading to the outlet. Near the midsection of the cavity closer to the right vertical wall, there is a strong downward flow. Possibly at this location, the fluid becomes cooler and hence denser and penetrates to the bottom to form a large clockwise recirculating region.

A slightly different behavior is seen in Fig. 5b for the cold jet ($Re = 50$, $Ri = -0.5$, $A = 1$). The left corner cell that appeared for $Ri = -0.1$ (Fig. 3b) has grown in size due to increased buoyancy. The cold fluid emanating from the top left corner sets up a recirculation region at the top. Some of the cold fluid descends downward and gets heated up by the right vertical

wall, and the buoyant force allows the fluid to move up again. Thus, a third cell appears in the case of high negative Richardson numbers.

Case studies were performed for $Re = 50$, $Ri = +0.5$ and aspect ratios of 0.5, 2.0, and 5.0, and some flow patterns and isotherms are presented. Figure 6 shows that for $A = 0.5$, the flow patterns for $Ri = 0.5$ and -0.5 are similar to those observed for $A = 1$ and $Ri = 0.1$ and -0.1. The cold jet ($Ri = -0.5$) as seen in Fig. 6b is able to penetrate to the bottom wall due to the small size of the cavity and effectively prevents the formation of a third cell. As expected, a secondary cell forms at the bottom right corner for $Ri = 0.5$. As the aspect ratio is increased to 2, the hot jet (not shown in the figure) is able to penetrate only to the middle of the cavity. The secondary cell is larger in size as in $A = 1$, although this cell originates from the right corner too.

The isotherms and vector velocity plots in Fig. 7 for $A = 2$ and $Ri = -0.5$ show that three cells are formed, as expected. No significant changes in the isotherm patterns were observed as aspect ratio was increased from 1 to 2; however, as seen in Fig. 7b, the secondary cells at the bottom occupy a larger portion of the cavity. As aspect ratio is further increased to 5 (Fig. 8) for the same Re ($=50$) and Ri ($=-0.5$), the flow patterns attain a vertical line of symmetry, with the downflow getting stronger.

The temperature profiles in the horizontal plane for both adiabatic and isothermal left walls are given in Fig. 9 in an effort to compare our results with those of Goldman and Jaluria.[1] In the experimental setup, perfect insulation on the left wall could not be achieved, and the bottom horizontal wall was removed. In this figure, the experimental data for $Re = 4500$ and $Ri = 0.007$ at a distance of 30ℓ from the jet exit shows a large scatter due to entrainment of ambient air. Since it is difficult to make direct comparisons of the present results with the experimental data, both adiabatic and isothermal left walls are considered at $Re = 2000$ and 4500 for $A = 5$. In the numerical study, the bottom wall is present. The numerical study predicts a higher temperature level in the fluid for the adiabatic left wall compared with that for an isothermal left wall for the same flow and geometric conditions. This was seen to be the case at different vertical positions. The temperature levels in the fluid for an adiabatic left wall are seen to be uniform at different vertical positions (Fig. 10), except close to the jet exit (a distance of 10ℓ from the jet exit), where a clear demarcation between the downward and the upward flow is noted by means of a hump in the profile. These general trends were also observed by Goldman and Jaluria.[1]

The wall friction factor and the heat-transfer rate on the bottom wall are presented in Fig. 11 for $A = 1$, $Re = 100$, and low Richardson numbers. The maximum Nu for cases with and without buoyancy occurs in between $x/1 = 2$ and $x/1 = 3$. This maximum is also found to decrease when the incoming jet is heated. The different cell patterns found in the flow earlier are consistent with the wall friction factor plotted in Fig. 11b. The negative friction factor indicates that the flow is in the opposite direction, and represents the corner cells. For $Ri = 0.1$ and -0.1, the absolute value of C_f^* reaches a maximum of approximately the same magnitude.

The effect of increased buoyancy is shown in Fig. 12. The heat-transfer rate and friction factor are negligible in the case of the hot jet. This is due to the inability of the jet to penetrate to the bottom of the cavity, setting up mild recirculating flow at the bottom. It is already seen that a triple cell pattern is observed for cold jets. Thus, the heat-transfer rate and friction factor are enhanced on the bottom wall for cold jets caused by the strengthened flow at impingement. The maximum value of Nu^* for $Ri = -0.5$ occurs when C_f^* is zero. As Reynolds number is increased to 200 (not shown in the figure), there is no significant shift in the location of the maximum Nu^*. However, the magnitude of the maximum increases.

As the depth of the cavity increases, in the case of cold jets, the initial momentum is not large enough to counter the buoyancy, and hence, the fluid cannot penetrate to the bottom of the cavity. The effect of aspect ratio on heat-transfer rate and friction factor is shown in Fig. 13. As the aspect ratio increases from $A = 0.5$ to 5 for cooled jets, the double-cell pattern changes into a triple-cell configuration, and the heat-transfer rate decreases. Figure 12a shows the maximum Nu^* occurring in the middle of the bottom wall for $A = 2$ and 5. However, as the aspect ratio is decreased, the maximum shifts to the left. Comparing Figs. 12a and 13a, it is clear that there exists another parameter in this problem, L/ℓ, which alters the flow situation and the heat-transfer rate. As the length of the bottom wall, L, is extended, the maximum heat-transfer rate shifts to the right, and the size of the left corner cell increases.

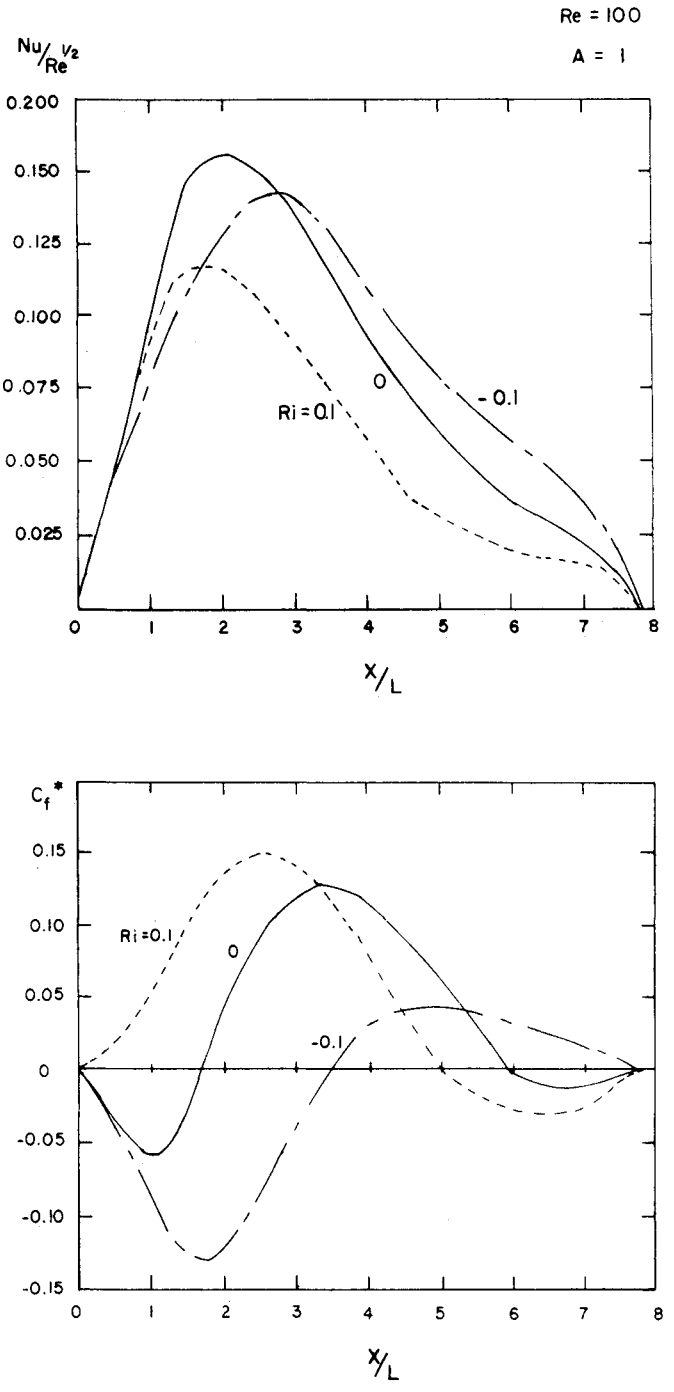

Fig. 11 Heat-transfer rate and friction factor for $Re = 100$, $A = 1$, and $Ri = 0$ (——), $Ri = 0.1$ (- - - -), and $Ri = -0.1$ (– – –).

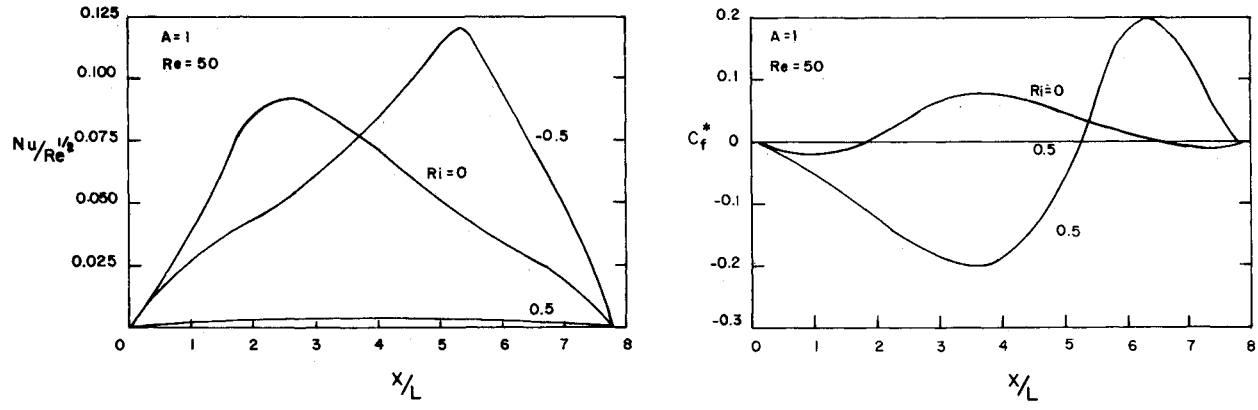

Fig. 12 Effect of high negative Richardson number on heat-transfer rate and friction factor; $Re = 50$, $A = 1$, and $Ri = 0$ and -0.5.

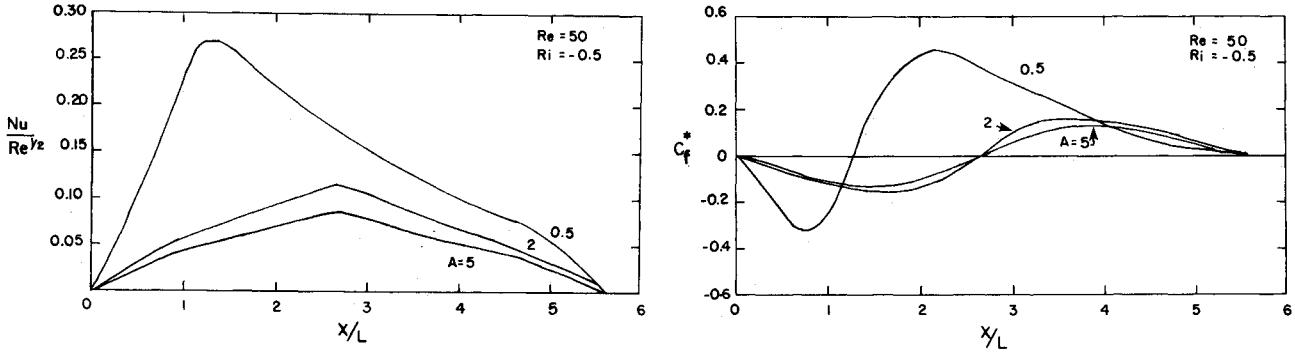

Fig. 13 Effect of aspect ratio on heat-transfer rate and friction factor; $Re = 50$, $Ri = -0.5$, and $A = 1$, 2, and 5.

Conclusions

The physics of the problem of a heated or cooled downward impinging jet in a cavity discharged from the other top corner of the cavity was examined by numerical analysis for a range of Reynolds and Richardson numbers, and aspect ratios. Buoyancy effects are found to be significant on the flow and thermal fields and the friction factor and heat-transfer rate.

The effect of a heated jet for low Richardson number Ri is to enhance the right corner eddy and remove the left corner eddy, and the opposite effect takes place for a cooled jet. When Ri is increased, the heated jet gives rise to a primary cell and a weak secondary cell that occupies about two-thirds of the cavity. For the same Ri, the cooled jet penetrates to the bottom of the cavity, the left-corner eddy is enhanced, and a strong right-corner eddy is developed. The cooler interior fluid accelerates vertically near the warmer walls.

As the aspect ratio is reduced, for cooled jets, the triple-cell configuration changes over to a primary eddy and a left-corner eddy, the flowfield loses its vertical symmetry, and the heat-transfer rate increases on the wall as a result of strengthened flow at impingement. The heat-transfer rate and friction factor become negligible as Ri is increased to 0.5 in cavities with $A > 1$ for heated jets. This is due to the inability of the jet to penetrate deep into the cavity. Another parameter, L/ℓ, is found to alter the flow situation and the magnitude and location of maximum heat-transfer rate. Further study is recommended to shed more light on the change in flow behavior with changes in jet width and the horizontal length of the cavity.

References

[1]Goldman, D. and Jaluria, Y., "Effects of Opposing Buoyancy on the Flow in Free and Wall Jets," *Journal of Fluid Mechanics*, Vol. 166, 1986, pp. 41–56.

[2]Cha, C. K. and Jaluria, Y., "Recirculating Mixed Convection Flow for Energy Extraction," *International Journal of Heat and Mass Transfer*, Vol. 27, 1984, pp. 1801–1812.

[3]Cha, C. K. and Jaluria, Y., "Effect of Thermal Buoyancy on the Recirculating Flow in a Solar Pond for Energy Extraction and Heat Rejection," *Journal of Solar Energy Engineering*, Vol. 106, 1984, pp. 428–437.

[4]Prahl, J., Ostrach, S., and Tong, T., "The Discharge of a Submerged Buoyant Jet into a Stratified Environment," *Proceedings of the Waste Heat Management Utilities Conference*, Vol. 3, VII-B, 1977, pp. 135–142.

[5]Satyanarayana, S. and Jaluria, Y., "A Study of Laminar Buoyant Jets Discharged at an Inclination to the Vertical Buoyancy Force," *International Journal of Heat and Mass Transfer*, Vol. 25, 1982, pp. 1569–1577.

[6]Turner, J. S., "Jets and Plumes with Negative or Reversing Buoyancy," *Journal of Fluid Mechanics*, Vol. 26, 1966, p. 779.

[7]Seban, R. A., Behnia, M. M., and Abreu, J. E., "Temperatures in a Heated Jet Discharged Downward," *International Journal of Heat and Mass Transfer*, Vol. 21, 1978, p. 1453.

[8]Yuan, T. D., Liburdy, J. A., and Wang, T., "Buoyancy Effects on Laminar Impinging Jets," *Proceedings of the ASME National Heat Transfer Conference*, HTD-Vol. 70, 1987, pp. 33–39.

[9]Torrance, K., Davis, R., Eike, P., Gill, P., Gutman, D., Hsui, A., Lyons, S., and Zien, H., "Cavity Flow Driven by Buoyancy and Shear," *Journal of Fluid Mechanics*, Vol. 51, Pt. 2, 1972, pp. 221–231.

[10]Patankar, S. V., *Numerical Heat Transfer and Fluid Flow*, Hemisphere, Washington, DC, 1980.

[11]Van Doormaal, J. P. and Raithby, G. D., "Enhancement of the SIMPLE Method for Predicting Incompressible Fluid Flows," *Numerical Heat Transfer*, Vol. 7, 1984, pp. 147–163.

[12]Howarth, L., "On the Calculation of the Steady Flow in the Boundary Layer Near the Surface of a Cylinder in a Stream," ARC RM 1632, 1935.